

Oligomeric structure of the *Bacillus subtilis* cell division protein DivIVA determined by transmission electron microscopy

H. Stahlberg,^{1†} E. Kutejová,^{2‡} K. Muchová,²
M. Gregorini,¹ A. Lustig,¹ S. A. Müller,¹ V. Olivieri,¹
A. Engel,¹ A. J. Wilkinson³ and I. Barák^{2*}

¹M. E. Müller Institute, Biozentrum, University of Basel, Klingelbergstrasse 70, CH-4056 Basel, Switzerland.

²Institute of Molecular Biology, Slovak Academy of Sciences, Dúbravská cesta 21, 845 51 Bratislava 45, Slovakia.

³Department of Chemistry, University of York, Heslington, York YO1 5OD, UK.

Summary

DivIVA from *Bacillus subtilis* is a bifunctional protein with distinct roles in cell division and sporulation. During vegetative growth, DivIVA regulates the activity of the MinCD complex, thus helping to direct cell division to the correct mid-cell position. DivIVA fulfils a quite different role during sporulation in *B. subtilis* when it directs the *oriC* region of the chromosome to the cell pole before asymmetric cell division. DivIVA is a 19.5 kDa protein with a large part of its structure predicted to form a tropomyosin-like α -helical coiled-coil. Here, we present a model for the quaternary structure of DivIVA, based on cryonegative stain transmission electron microscopy images. The purified protein appears as an elongated particle with lateral expansions at both ends producing a form that resembles a 'doggy-bone'. The particle mass estimated from these images agrees with the value of 145 kDa measured by analytical ultracentrifugation suggesting 6- to 8-mers. These DivIVA oligomers serve as building blocks in the formation of higher order assemblies giving rise to strings, wires and, finally, two-dimensional lattices in a time-dependent manner.

Introduction

The molecular mechanisms of cell division have been studied intensively for several decades, the best charac-

terized systems being those operating in the rod-shaped bacteria *Escherichia coli* and *Bacillus subtilis*. Despite these efforts, many basic questions remain unanswered. For example, the mechanism that ensures the correct placement of the division septum, a key aspect of bacterial cell division, is only partly understood. The protein FtsZ plays a pivotal role in the temporal and spatial control of symmetric division at the mid-cell site in almost all bacteria, as well as division at polar sites in bacteria that divide asymmetrically during their life cycle. FtsZ is homologous to the eukaryotic tubulins and forms cytokinetic rings (Z-rings) at the sites of cell division (Bi and Lutkenhaus, 1991). Z-ring formation is the earliest known step in bacterial cell division and takes place well before cell membrane invagination and complete nucleoid separation (Bi and Lutkenhaus, 1991).

FtsZ-ring formation, and thus the selection of the site of division, is controlled by at least two mechanisms: nucleoid occlusion and inhibition by the Min system (Harry, 2001). The nucleoid occlusion model states that the nucleoid has a negative effect on division wherever it occupies space in the cell. Thus, the mid-cell site appears and disappears cyclically during vegetative growth with rounds of chromosome replication (Errington *et al.*, 2003). Although the nucleoid occlusion model (Woldringh *et al.*, 1991) is very attractive, it is still poorly defined.

A principal function of the Min system is to prevent division at the cell poles. In *E. coli*, it comprises three components, MinC, MinD and MinE. MinC and MinD form a complex that prevents cell division by inhibiting FtsZ polymerization and Z-ring formation. MinE is a topological factor allowing relief of division inhibition in the central region of the cell (de Boer *et al.*, 1992). Recent localization experiments in living cells have revealed that MinD, which is a membrane-associated ATPase (de Boer *et al.*, 1991), oscillates from pole to pole (Raskin and de Boer, 1999a,b). The period of this remarkable oscillation is 10–20 s. The division inhibitor MinC is also observed to oscillate from pole to pole and, as it oscillates with the same pattern as MinD, and only does so in the presence of MinD, the proteins probably co-oscillate as a MinC–MinD complex (Hu and Lutkenhaus, 1999; Raskin and de Boer, 1999a). MinE was originally thought to form a mid-cell, ring-like structure, defining the site of subsequent FtsZ-ring assembly (Raskin and de Boer, 1997). However, in

Accepted 4 February, 2004. *For correspondence. E-mail imrich.barak@savba.sk; Tel. (+421) 2 5930 7418; Fax (+421) 2 5930 7416. †Present address: Molecular and Cellular Biology, UC-Davis, CA 95616, USA. ‡These authors contributed equally to this work.

living cells, MinE also undergoes a rapid oscillation coupled to that of MinD and MinC (Fu *et al.*, 2001). The oscillating movements of MinD and MinE are mutually dependent, because lack of MinE leads to a uniform distribution of the MinCD complex around the cytoplasmic membrane (Rowland *et al.*, 2000). In addition, it has been shown recently that the three Min proteins are organized into extended membrane-associated coiled structures that wind around within the cell between the two poles (Shih *et al.*, 2003). Thus, the pole-to-pole oscillation of the proteins reflects oscillatory changes in their distribution within the coiled structure.

Although the cell division processes in *E. coli* and *B. subtilis* are fundamentally similar, Bacilli appear to use a different strategy in initiating mid-cell division. *B. subtilis* has MinCD homologues but lacks a MinE counterpart, and the MinCD complex does not oscillate between the cell poles. Instead, MinCD is recruited to the division site by a 19.5 kDa cytoplasmic protein, DivIVA (Cha and Stewart, 1997; Edwards and Errington, 1997; Marston *et al.*, 1998). DivIVA has no sequence similarity to MinE, and the two proteins function differently (Zhang *et al.*, 1998). DivIVA forms large oligomers (Muchova *et al.*, 2002), whereas MinE is a dimer (Zhang *et al.*, 1998).

Comparison of the ways in which Gram-negative and Gram-positive bacteria regulate mid-cell site selection during binary fission reveals that fundamentally different schemes have evolved. Binary fission involves not only identification of the mid-cell and the construction of a septum at this site, but also rejection of other (polar) sites for the assembly of the cell division apparatus. In addition to nucleoid occlusion, which probably pertains in all bacteria, prokaryotes also control division site selection using the Min system. This system seems to have evolved in three basic ways: through MinE oscillation, through DivIVA regulation and by a third uncharacterized mechanism. The latter conclusion is based on the observation that bacterial species such as *Caulobacter*, *Mycoplasma* and *Haemophilus* lack recognizable Min homologues (Margolin, 2001). However, completed genome sequence data suggest that the problem is more complicated. In *Clostridium acetobutylicum* and *Clostridium difficile*, both *minE* and *divIVA* genes are present (Stragier, 2001), although it is not established whether *minE* is functional in these organisms and how it and *divIVA* contribute to mid-cell site selection.

The *B. subtilis* DivIVA/MinCD division system appears to have no direct role in the initiation of FtsZ-ring formation at the mid-cell site; rather, it inhibits division at the polar sites. DivIVA has another function during endospore formation, a developmental process that begins with an asymmetric septation, giving rise to a larger mother cell and a smaller prespore. In this process, the role of DivIVA is not in regulation of division site selection; instead, it

functions in prespore chromosome segregation (Thomaidēs *et al.*, 2001). Taken together, the main roles of DivIVA seem to be (i) to direct the MinCD complex to polar sites during vegetative growth; and (ii) through direct or indirect interaction with RacA, to help to anchor chromosomes to the poles during sporulation (Ben-Yehuda *et al.*, 2003; Wu and Errington *et al.*, 2003). As DivIVA may interact with alternative proteins, as mentioned above, it is possible that their competition somehow triggers polar division.

In this paper, we present the quaternary structure of a biologically active variant of DivIVA (DivIVA9) determined by cryonegative stain transmission electron microscopy (TEM). The experiments demonstrate that elongated protein particles as small as 130 kDa can be imaged individually, using cryonegative stain TEM. The possible contributions of these DivIVA structures to its biological function are discussed with the aim of explaining the extraordinary manner in which this protein recognizes the cell poles.

Results

DivIVA and its mutant derivatives expression, isolation and purification

All experiments were performed with two different mutant variants of DivIVA, DivIVA9 and DivIVA2, described previously by Muchova *et al.* (2002). The Glu-162Lys and Leu-120Pro substitutions giving rise to DivIVA9 and DivIVA2, respectively, were acquired during attempts to overexpress recombinant DivIVA in *E. coli*. The *divIVA9* gene is stable in the *E. coli* expression system in contrast to the wild-type *divIVA* gene, which acquires mutations and deletions (Muchova *et al.*, 2002). In *B. subtilis*, the *divIVA9* allele does not cause any detectable defects in cell growth or morphology. Thus, it is reasonable to assume that wild-type DivIVA and DivIVA9 are functionally and structurally similar proteins.

DivIVA9 was purified by Q Sepharose Fast Flow, Mono Q and gel filtration chromatography as described in *Experimental procedures*. The retention volume of the protein on the gel filtration column suggests a species with a molecular weight somewhere between those of the 158 kDa and 2000 kDa standards (Fig. 1). A very similar gel filtration profile was observed with a hexahistidine-tagged derivative of DivIVA9 (not shown). Purified DivIVA9 precipitates if stored at -20°C even in 10% glycerol. At high protein concentrations, it also precipitates at 4°C (Muchova *et al.*, 2002). Indeed, at a concentration of 10 mg ml^{-1} , DivIVA9 precipitates from solution over a period of several minutes at 4°C . At the lower concentration of 4 mg ml^{-1} , precipitation is much slower, taking place over several days.

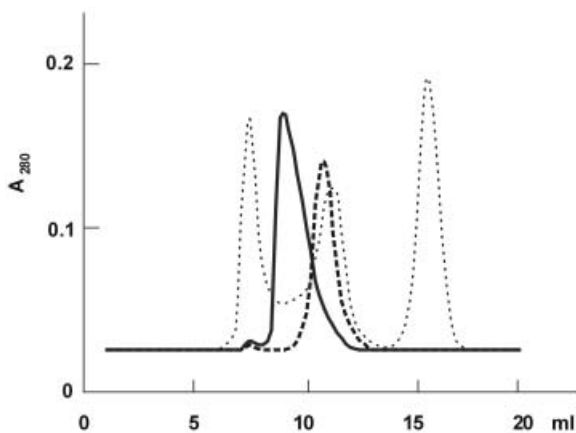


Fig. 1. Superose 12 gel filtration chromatograms of DivIVA proteins. The continuous line represents DivIVA9 and the dashed line His₆-tagged DivIVA2. In each experiment, a 0.5 ml sample was loaded containing either DivIVA9 at 2.6 mg ml⁻¹ or His₆-tagged DivIVA2 at 2.2 mg ml⁻¹. The dotted line is the chromatogram of molecular weight standards: blue dextran (2000 kDa), aldolase (158 kDa) and cytochrome C (12.5 kDa).

The second mutant protein, DivIVA2, which is associated with severe defects in cell division and sporulation (Muchova *et al.*, 2002), was isolated as a hexahistidine-tagged form on a Ni-NTA agarose column. Its retention volume on the Superose 12 column was significantly higher than that of DivIVA9 and its hexahistidine-tagged derivative, suggesting a much smaller species. Together, the results imply that there is a significant difference between the oligomeric states of DivIVA9 and DivIVA2. This difference in the quaternary structure of the proteins may correlate with the different *in vivo* effects of the *divIVA9* and *divIVA2* alleles.

Transmission electron microscopy imaging of DivIVA9 and DivIVA2 mutant proteins

TEM of samples quick frozen in the presence of an ammonium molybdate stain (Adrian *et al.*, 1998) was used to analyse DivIVA immediately after purification and at a series of later times. In other TEM experiments, either unstained cryosamples in fenestrated carbon film (Dubochet *et al.*, 1988) or samples negatively stained with uranyl acetate or phosphotungstic acid (PTA) were prepared and examined. Unstained cryo TEM was unable to produce usable images of DivIVA, because of the small size and weight of the complexes. Although faint elongated particles could be observed in the negatively stained TEM samples imaged at room temperature (data not shown), the better resolution and signal-to-noise ratio of images obtained by cryonegative stain TEM were needed for the oligomeric protein structures to be visualized clearly.

Cryonegative stain TEM images of freshly purified

DivIVA9 samples showed the presence of elongated particles with lateral expansions at both ends, making them resemble in some sense 'doggy-bones'. These particles were observed in all samples imaged within 1–3 days of protein purification (Fig. 2A–C). The flexible structures have a length of 22.4 ± 3.0 nm and a width of 2.9 ± 0.3 nm ($n = 16$). In contrast, TEM images of His-tagged DivIVA2 samples revealed diffuse objects without distinct shape, and there was no evidence of aggregation even after the stock had been stored for several days at 8°C (Fig. 2D). When stored in the same way, DivIVA9 aggregates slowly (see below).

To examine the possibility of further DivIVA9 oligomerization, cryonegatively stained samples were prepared after storage of the protein for up to 5 days at 8°C. Although samples stored for 2 days contained single 'doggy-bone'-shaped particles (Fig. 2), the TEM images of samples prepared at later time points showed higher order structures (Fig. 3). The end-to-end oligomerization of two 'doggy-bone'-shaped particles was frequently observed (Fig. 3A). The end-to-end contacts of the 'doggy-bones' sometimes had a slight lateral displacement. We also observed 'strings' of linearly associated doggy-bone particles, laterally associated strings forming thin 'wires' (Fig. 3B) and two-dimensional networks of doggy-bone particles (Fig. 3C). These exhibit the same contrast as the individual 'doggy-bone' particles, suggesting that the networks are single-layered two-dimensional ribbons rather than three-dimensional bundles. The Fourier transform computed for the marked region of the two-dimensional network shown in Fig. 3C is displayed in the inset. The diffraction spots prove the existence of an ordered real-space lattice in the image, with two-dimensional crystal dimensions of $u = 24$ nm, $v = 10$ nm and an opening angle, α of 117°. Sometimes two-dimensional networks with neighbouring 'doggy-bone' particles displaced along the longer crystal axis were observed. In these instances, the ends of some DivIVA particles establish contact not with the ends but with the centres of others (Fig. 4C). Older samples frequently showed mixtures of different oligomeric forms, and the incidence of the higher order oligomers was higher than before storage. This higher order oligomerization could be reversed by the addition of 200 mM (NH₄)₂SO₄ and incubation for 1 h at 8°C before sample preparation. Subsequent TEM imaging then again revealed mostly individual 'doggy-bone'-shaped particles. In the presence of 200 mM (NH₄)₂SO₄, the non-aggregated 'doggy-bone' complex was stable for several days at 8°C (Fig. 2B).

Estimation of oligomerization state of DivIVA9 by analytical ultracentrifugation

To determine the oligomerization state of the DivIVA9

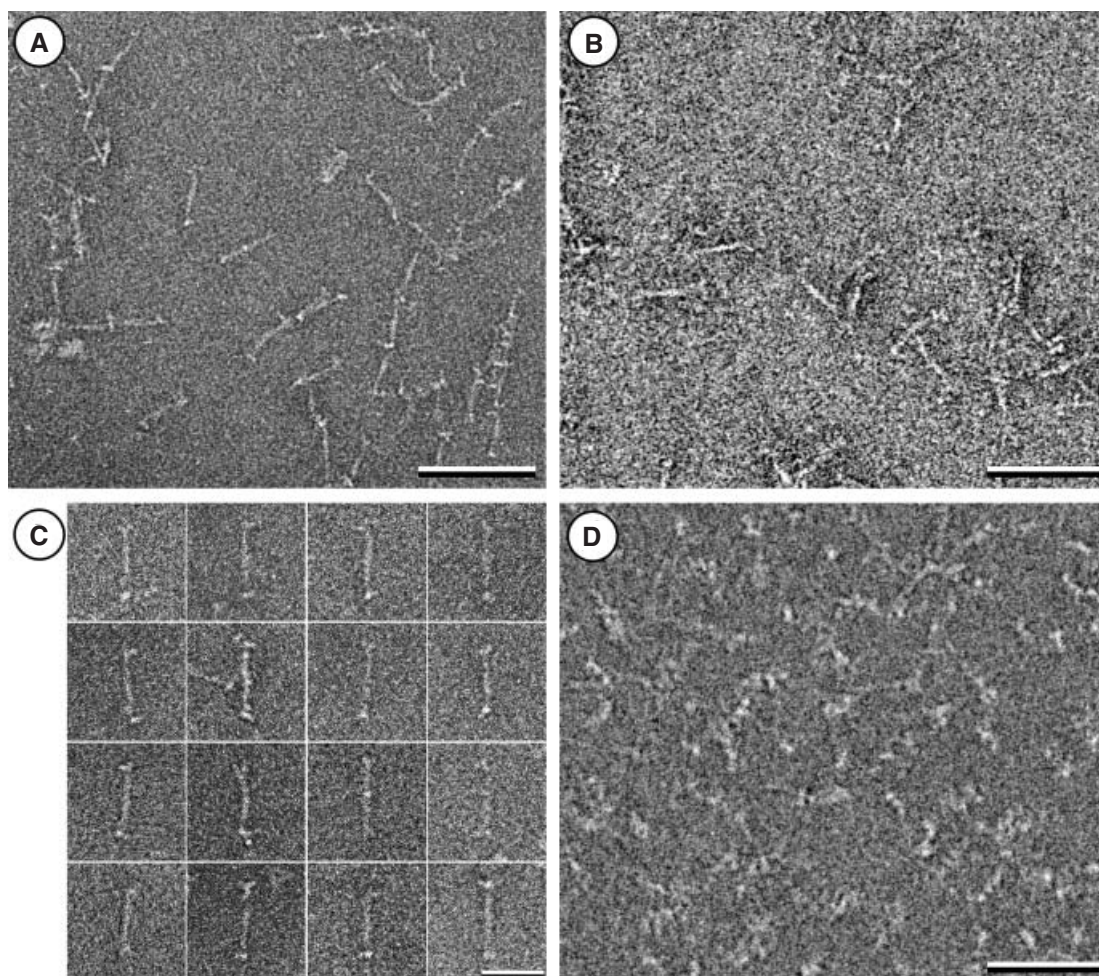


Fig. 2. Cryonegative stain TEM images of DivIVA.

A. DivIVA9, freshly purified and imaged within 2 days.

B. DivIVA9, purified and stored for 3 days at 8°C in 200 mM $(\text{NH}_4)_2\text{SO}_4$.

C. Examples of 'doggy-bone'-shaped particles, as found in (A) and (B).

D. Cryonegative stain image of His6-tagged DivIVA2 that had been purified and subsequently stored for 5 days at 8°C.

Scale bar for (A), (B) and (D) is 50 nm; for (C) is 20 nm.

'doggy-bones', sedimentation measurements were made in the analytical ultracentrifuge (AUC). The experiments were carried out in ammonium sulphate buffer as described in *Experimental procedures*. A single sedimentation velocity (SV) run at a protein concentration of 0.4 mg ml^{-1} revealed a single boundary with an $S_{20,W}$ value of 2.7. Several sedimentation equilibrium (SE) runs at 10 000 and 14 000 r.p.m. made over a protein concentration range of 0.4 mg ml^{-1} to 0.1 mg ml^{-1} showed a strong concentration dependence of the measured mass, which varied from 104 kDa to 134 kDa. The extrapolated molecular weight at a concentration of zero mg ml^{-1} was $145 \pm 10 \text{ kDa}$. The ratio of the frictional coefficient (f) calculated for the protein concentration of 0.4 mg ml^{-1} ($M = 104 \text{ kDa}$, $s = 2.7 \text{ S}$) to that of a rigid sphere (f_0) was 2.95 with a hydrodynamic radius of

9.2 nm. A value for f/f_0 of 1 corresponds to an ideal spherical-shaped protein. The extremely high f/f_0 value obtained for DivIVA9 indicates that the particle shape has a high aspect ratio. The AUC results suggest that the DivIVA9 protein forms elongated 6- to 8-mers under the conditions used. This observation is in contrast to our previous AUC results, which suggested that the mass of DivIVA9 increases from that expected for a dimer to one corresponding to a 12-mer (Muchova *et al.*, 2002). The possible explanation for the observed discrepancy might be the use of different buffers in the two experiments. As documented by the TEM experiments, ammonium sulphate disrupts the end-to-end contact of pairs of 'doggy-bone' particles, which would lead to the 10- to 12-mer observed previously in AUC experiments (Muchova *et al.*, 2002).

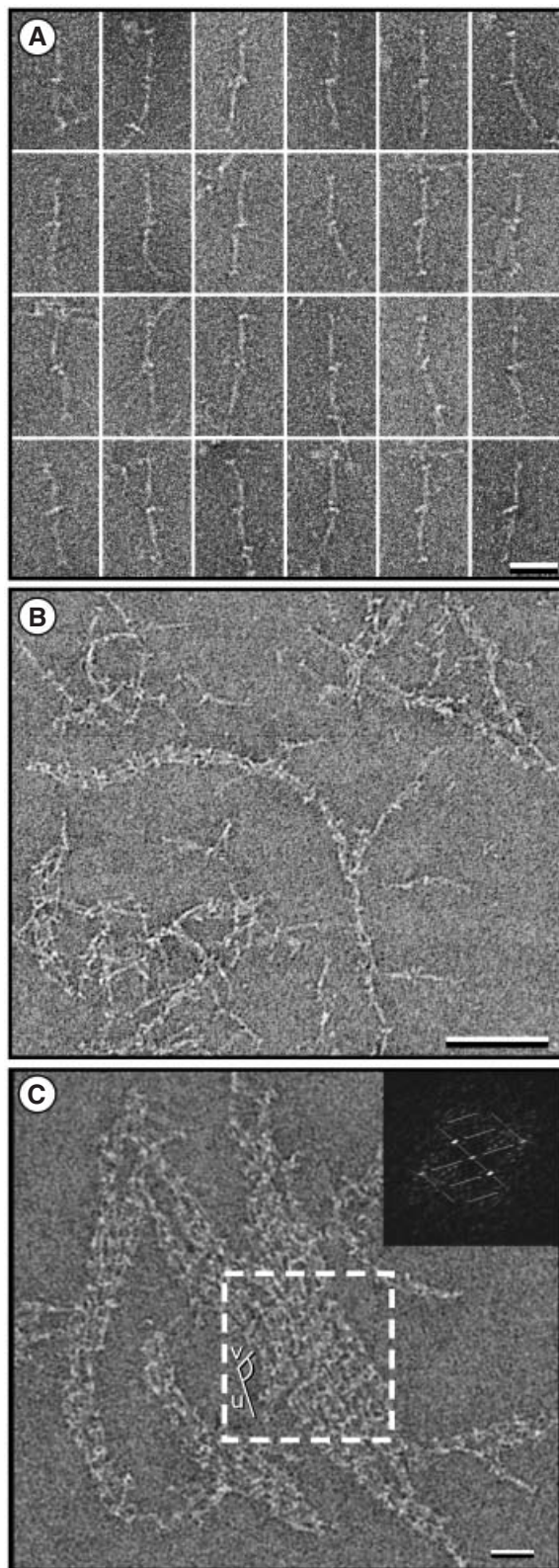


Fig. 3. Cryonegative stain TEM images of DivIVA9, stored at 8°C in the absence of $(\text{NH}_4)_2\text{SO}_4$.

A. Examples of 'doggy-bone' pairs that can frequently be observed 2 days after purification.

B. Three days after purification; the 'doggy-bone'-shaped particles arrange in 'strings'.

C. After 5 days; two-dimensional networks are formed. The indicated area of the two-dimensional network shown was computationally Fourier transformed. The corresponding power spectrum is reproduced in the inset (top right), revealing the presence of a real-space lattice with dimensions $u = 24$ nm, $v = 10$ nm, $\alpha = 117^\circ$. These real-space lattice vectors are indicated in the image.

Scale bar for (A) is 20 nm; for (B) is 50 nm; and for (C) is 20 nm.

Oligomerization state of the 'doggy-bone' structures indicated by microscopy

As noted above, the 'doggy-bone' complexes evident on TEM images recorded from purified DivIVA9 samples were 22.4 ± 3.0 nm long and 2.9 ± 0.3 nm wide. A cylindrical rod of the same length and diameter would have a volume of 145 ± 31 nm³. Taking the average density of protein to be 810 Da nm⁻³, this would correspond to a mass of 117 ± 24 kDa. Taking into account the lateral expansions at both ends, this is in agreement with the 'doggy-bone' being a DivIVA9 6- to 8-mer (monomer mass of 19.5 kDa). It is probable that the DivIVA9 protomers are in extended conformations, spanning the length of the 'doggy-bone'. DivIVA9 has 164 amino acid residues. If these take up the anticipated extended α -helical structure, they would have a length 24.6 nm, in good agreement with the length of the long axis of the 'doggy-bone'.

The scanning transmission electron microscope (STEM) was used in a further series of experiments aimed at measuring directly the mass of the 'doggy-bone' complexes. The microscopy grids were prepared using material that had been stored for a period of weeks in the presence of 200 mM $(\text{NH}_4)_2\text{SO}_4$ at 8°C. Images recorded from negatively stained (PTA) samples using the STEM documented the continued presence of elongated particles (data not shown). In the absence of stain, the elongated structures could only rarely be distinguished with certainty, and attempts to measure their mass failed to give a statistically representative result. Nevertheless, the mass of 63 elongated particles <26 nm long could be estimated roughly and was 133 ± 62 kDa. The mass-per-length (MPL) could also be determined for 42 of these, being 3.6 ± 1.7 kDa nm⁻¹ ($n = 41$) and 9.6 kDa nm⁻¹ ($n = 1$). Although of little statistical significance, the results imply that the ≈ 22 -nm-long 'doggy-bone' particles imaged by TEM were not DivIVA dodecamers, as indicated earlier by AUC experiments made in the absence of $(\text{NH}_4)_2\text{SO}_4$ (Muchova *et al.*, 2002). Further, the MPL of ≈ 4 kDa nm⁻¹ measured for some of the elongated particles supports a hexameric stoichiometry (expected value 4.8 kDa nm⁻¹ assuming the above conformation).

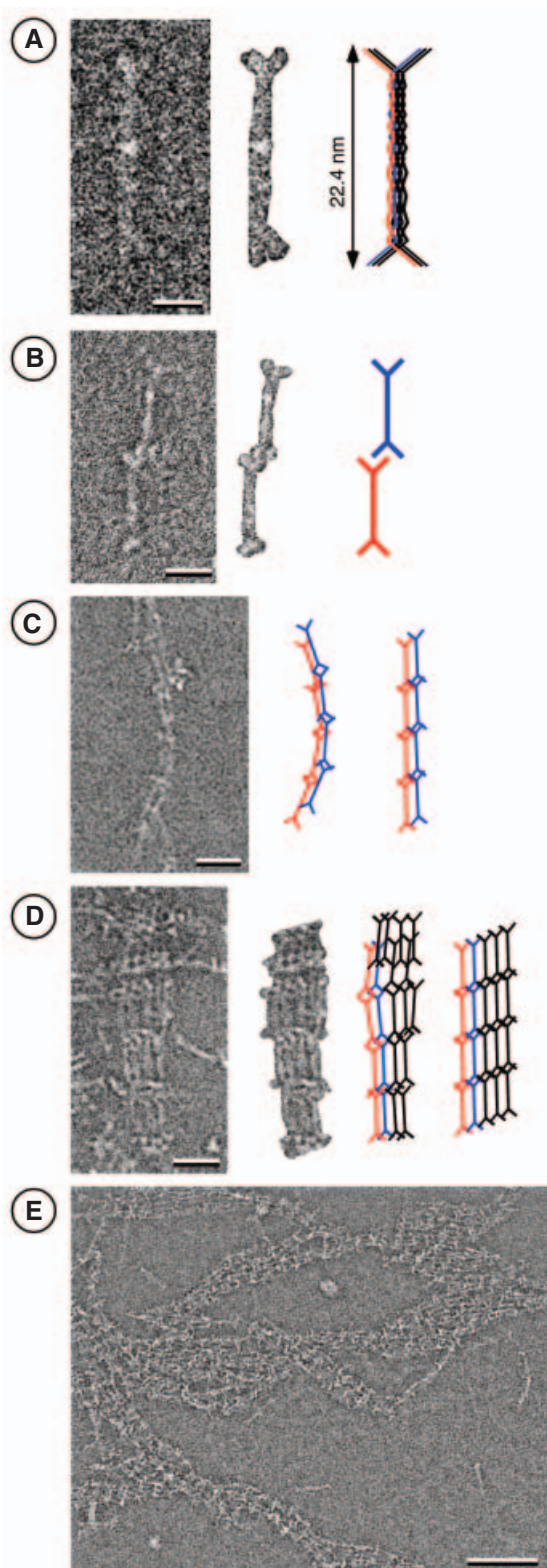


Fig. 4. Tentative scheme of DivIVA9 oligomerization.

A. Freshly purified DivIVA9 appears as 'doggy-bone'-shaped particles 22.4 ± 3 nm long and 2.0 ± 0.4 nm wide (left). A masked particle is reproduced to guide the reader's eyes (centre). A tentative model for the hexameric oligomer (right).

B. 'Doggy-bone' particles oligomerize end to end to form pairs. A lateral displacement was sometimes observed, as in the example shown (left). Masked particle (centre). Model (right).

C. Further end-to-end oligomerization gives rise to 'strings'.

D. Several strings attach laterally in a plane to form thin 'wires' (left). Models (centre and right).

E. Further aggregation leads to two-dimensional network formation. Scale bar for (A) is 5 nm; for (B) is 10 nm; for (C) and (D) is 20 nm; and for (E) is 50 nm.

Discussion

In this study, TEM images of DivIVA9 revealed 'doggy-bone'-shaped oligomers that further assemble into two-dimensional networks. As the *divIVA9* allele has no effect on cell division and sporulation (Muchova *et al.*, 2002), it is reasonable to propose that wild-type DivIVA forms the same oligomers and networks as DivIVA9. In contrast, the His₆-tagged DivIVA2 protein, which fails to form 'doggy-bone'-shaped oligomers, severely impairs these processes in *B. subtilis*. The His₆-tagged form of DivIVA9 showed the same behaviour in gel filtration experiments as the untagged protein (Fig. 1), indicating the formation of similarly elongated particles as observed for DivIVA9. These experiments, as well as previous characterization of untagged DivIVA2 (Muchova *et al.*, 2002), suggest that, in this mutant, the failure to oligomerize like DivIVA9 is not caused by the presence of the His₆ tag. According to the AUC results, the 'doggy-bone' complexes are formed by six to eight copies of the 19.5 kDa DivIVA9 protein.

The elongated shape of the 'doggy-bone' complex (22.4 ± 3.0 nm long and 2.9 ± 0.3 nm wide) explains the discrepancy between the molecular mass estimated from the gel filtration experiments and that measured by AUC. Being an elongated particle, DivIVA9 elutes at a much lower volume than a spherical particle of equivalent mass (Fig. 1).

A scheme for the oligomerization of DivIVA is presented in Fig. 4, in which masked particles from the cryonegative stain TEM images are shown alongside tentative models of the 'doggy-bone' oligomer and its assemblies. Our data indicate that 'doggy-bone' aggregation starts with the formation of end-to-end dimers (Fig. 4B). This would account for the 10- to 12-mers seen previously in AUC experiments run in the absence of ammonium sulphate (Muchova *et al.*, 2002). Oligomerization continues with the formation of 'strings', thin 'wires' (Fig. 3C) and two-dimensional 'networks' (Fig. 4D and E). As indicated at the upper end of the model in Fig. 4D, DivIVA 'doggy-bones' occasionally establish end-to-centre contacts, giving rise to staggered two-dimensional networks in which neighbouring oligomers are displaced along their long crystal axis.

The observed oligomerization is unlikely to have been influenced by the cryonegative stain sample preparation method, as network formation is time dependent. Further, as the 'doggy-bone'-shaped DivIVA9 particles are building blocks for the higher aggregates, this conformation must exist in solution and cannot be an artifact of the 30 s exposure to ammonium molybdate during the staining procedure.

The oligomerization and lattice-forming properties exhibited by DivIVA9 in this study may be significant for the biological function of the wild-type protein. Other cell division proteins form two-dimensional or three-dimensional networks, the best known example being FtsZ. FtsZ forms Z-rings at sites of septation (Bi and Lutkenhaus, 1991), although in *B. subtilis*, it can also appear in the form of spirals as the Z-ring migrates from the mid-cell site to the two polar positions at the beginning of sporulation (Ben-Yehuda and Losick, 2002). FtsZ has a strong propensity to polymerize in a GTP-dependent manner *in vitro*, forming structures that include sheets and filaments (Bramhill and Thompson, 1994). FtsZ is a weak homologue of tubulin, which forms microfilamentous structures that provide either a track along which proteins can be translocated or an anchor to which proteins of the cytoskeleton of eukaryotic cells can attach. Interestingly, DivIVA is a homologue of tropomyosin, an actin-binding protein that forms coiled-coil filaments (Whitby *et al.*, 1992). The highly ordered oligomeric structures formed by DivIVA may be crucial for anchoring different proteins, enabling DivIVA to control complex processes such as cell division and sporulation in Gram-positive bacteria.

The ability of DivIVA to form 6- to 8-mers and two-dimensional networks may be crucial for both vegetative and asymmetric cell division. Harry and Lewis (2003) and Hamoen and Errington (2003) have shown that DivIVA localization to the poles is independent of FtsZ localization. However, a dependence of DivIVA localization on the mid-cell localization of FtsZ and other division proteins including DivIB, DivIC (Marston *et al.*, 1998) and PBP 2B (Daniel *et al.*, 2000; Hamoen and Errington, 2003) has been reported previously. How DivIVA oligomers become sequestered to the polar sites is not yet known. The requirement of FtsZ and PBP 2B for polar targeting of DivIVA during vegetative growth seems to be indirect and probably only arises because of their role in the formation of the new cell pole. The polar localization of DivIVA is also independent of the cytoskeletal proteins Mbl and MreB (Hamoen and Errington, 2003). Taken together, it seems that, in contrast to mid-cell localization, polar localization of DivIVA does not need any known cell division or cytoskeletal protein. Similarly, the DivIVA homologue from *Streptomyces coelicolor* specifically recognizes hyphal tips in a septation-independent manner enabling it to either establish or maintain the cell polarity that is

needed for tip extension (Flårdh, 2003). It is possible that DivIVA can recognize some general feature of cell poles as *B. subtilis* DivIVA can target poles in both *E. coli* and *Schizosaccharomyces pombe*, neither of which have DivIVA-like proteins (Edwards *et al.*, 2000). These observations suggest an intriguing function for DivIVA-like proteins as morphogenes capable of creating the cell polarity needed for sporulation in *B. subtilis*, tip extension in *S. coelicolor* and/or polar growth in many actinomycetes.

Our results suggest tentative structural explanations for how DivIVA recognizes the cell poles. One possibility is that the two-dimensional DivIVA networks specifically recognize some characteristic of the cell's morphology, for example by developing a curvature that precisely matches that of the cell poles. Another possibility is that DivIVA oligomers are directed to the poles by recently proposed 'activity-based structures', or hyperstructures, in which various types of molecule are brought together to perform a function at a specific part of the membrane (Norris *et al.*, 2002a,b). Such hyperstructures may be responsible for differentiating the membrane at the cell pole from the rest of the cell membrane, so providing a means of controlling cell processes such as DNA replication and cell division. Subsequently, DivIVA sequesters other specific proteins to these sites. These hypotheses may have a great impact on our understanding of how bacterial proteins can be targeted to specific sites by recognizing physical characteristics of cell shape.

Experimental procedures

Bacterial strains and plasmids

Escherichia coli MM294 (Backman *et al.*, 1976), BL21(DE3) (Novagen), IB706 (Muchova *et al.*, 2002), IB884 (this work) and IB886 (this work) strains were grown in Luria-Bertani (LB) rich medium supplemented with 100 µg ml⁻¹ ampicillin or 30 µg ml⁻¹ kanamycin where appropriate. pET15IVA2 and pET15IVA9 plasmids were constructed by ligating the *divIVA2* and *divIVA9* coding sequences from pETIVA2 and pETIVA9, respectively (Muchova *et al.*, 2002), into pET-15b (Novagen) at the *NdeI* and *BamHI* sites. The resulting recombinant plasmids were used to transform *E. coli* BL21 (DE3) to create strains IB884 and IB886 respectively.

Isolation and purification of DivIVA9 protein

The isolation and purification of DivIVA9 was carried out essentially as reported previously (Muchova *et al.*, 2002). Briefly, 3.5 g of IB706 cells in 10 ml of buffer A [50 mM Tris-HCl, pH 8.0, 100 mM NaCl, 1 mM EDTA, 1 mM dithiothreitol (DTT), 1 mM AEBSF] was lysed by sonication, and the cell debris was removed by centrifugation at 100 000 *g* for 30 min. The supernatant was applied to a 13 ml Q Sepharose Fast Flow column (Pharmacia Biotech), and DivIVA9 was eluted with a 91 ml of 0.1–0.4 M NaCl linear gradient in buffer A. Fractions containing DivIVA9 were diluted fivefold with buffer A and loaded on to an FPLC Mono Q HR 10/16 column

(Pharmacia Biotech), which was developed with a 70 ml 0.1–0.3 M NaCl gradient in buffer A. DivIVA9 fractions were concentrated by Centricon K10 filtration and loaded (500 µl) on to a Superose 12 column (Pharmacia Biotech). Pure DivIVA9 fractions were then either used directly for electron microscopy studies or concentrated to 0.4 mg ml⁻¹. For the AUC and for some TEM experiments, (NH₄)₂SO₄ (pH 8.0) was added to a final concentration of 0.2 M. All procedures were carried out at 4°C. DivIVA9 protein with a His₆ tag at its N-terminus was isolated as for the His-tagged DivIVA2 (see below).

Isolation and purification of DivIVA2 protein

Because of the instability of DivIVA2, this mutant was isolated with a His₆ tag at the N-terminus using Ni-NTA agarose chromatography. A sample of 3.5 g of induced IB884 cells in 10 ml buffer A was lysed by sonication, and the soluble fraction was collected after centrifugation at 200 000 *g* for 12 min. The supernatant was applied to a 1 ml Ni-NTA agarose (Qiagen) column. After washing the column with 5 ml of 40 mM imidazole in buffer B (20 mM Tris-HCl, pH 8.0, 150 mM NaCl, 20% glycerol), His₆-tagged DivIVA2 was eluted with 0.3 M imidazole in buffer B and desalted on a NAP5 column (Pharmacia Biotech) into buffer A. All procedures were carried out at 4°C.

Analytical ultracentrifugation

Analytical ultracentrifugation analysis was performed on purified DivIVA9 samples in 20 mM Tris-HCl, pH 8.0, 200 mM (NH₄)₂SO₄, 100 mM NaCl. Sedimentation velocity (SV) and sedimentation equilibrium (SE) runs were carried out in a Beckman XLA analytical ultracentrifuge, equipped with absorption optics. The SV runs were performed at 54 000 r.p.m. and 20°C using a 12 mm double-sector cell. The SE runs were made at 10 000 and 14 000 r.p.m., 20°C and scanned at two wavelengths, 278 nm and 230 nm. The SE results were analysed using a floating baseline computer program that adjusts the baseline absorbance to obtain *lnA* versus *r*², where *A* is the absorbance and *r* the radial distance. A partial specific volume of 0.73 cm³ g⁻¹ and a solution density of ρ = 1.012 g cm⁻³ was used. A solution viscosity of 1.02 centipoise was taken for the conversion of *S* to *S*_{20,w}. The total conversion factor including the solution density was 1.05.

Transmission electron microscopy

The purified DivIVA sample was prepared for cryonegative stain TEM as described previously (Adrian *et al.*, 1998). A 3 µl drop of the sample was put on a TEM grid that had been coated with a fenestrated carbon film. This grid was then placed face down on a drop of 100 µl of saturated ammonium molybdate solution, pH 7.5, for 30 s. The grid was then blotted, quick-frozen in liquid ethane-cooled liquid nitrogen and transferred with a Gatan-626 cryoholder into a Philips CM200FEG microscope operated at 120 kV or 200 kV. Images were recorded at nominal magnifications of 50 K× to 115 K× on Kodak SO-163 photographic film, which was subsequently developed for 12 min in full-strength developer. The negatives were scanned into a computer with a Heidelberg Primescan 7100 for further processing.

Scanning transmission electron microscopy

The mass measurements were made on a DivIVA9 sample that had been stored in the presence of 200 mM ammonium sulphate for several weeks at 8°C. The sample was diluted 1:3 with quartz double-distilled water, after which a 7 µl aliquot was adsorbed to a STEM microscopy grid: a gold-coated copper grid covered by a thick fenestrated carbon film and, finally, a thin carbon layer. The grid was then washed on four drops of quartz double-distilled water and freeze dried overnight in the microscope. The sample was diluted by the same amount for the negative stain STEM, and the grid was prepared similarly except that the water washes were omitted. Instead, the grid was negatively stained on two droplets of 2% uranyl acetate and air dried.

A Vacuum Generators STEM HB-5 interfaced to a modular computer system (Tietz Video and Image Processing Systems) was used. The darkfield images required for mass measurement were recorded from the unstained sample at an accelerating voltage of 80 kV. The nominal magnification was 200 K×. Recording doses were in the range of 1000 electrons nm⁻². The 512 × 512 pixel digital images were evaluated using the program package IMPSYS as outlined previously (Müller *et al.*, 1992; Lupas *et al.*, 1995). The mass-per-length, evaluated from images recorded on the same day from tobacco mosaic virus (kindly supplied by Dr R. Diaz-Avalos, Institute of Molecular Biophysics, Florida State University, Tallahassee, FL, USA) adsorbed to a separate grid, served as a calibration standard. Further, the DivIVA9 data were corrected for beam-induced mass loss based on the behaviour of four proteins with an average mass of 159 ± 32 kDa. Subsequently, the mass values were displayed in histograms and described by Gauss curves.

Images were recorded from the negatively stained sample at the nominal magnification of 200 K× and 80 kV accelerating voltage.

Acknowledgements

This work was supported by Wellcome Trust grants (numbers 066732/Z/01/Z to I.B. and A.J.W. and 057339/Z/99/Z to A.J.W.), a grant from the Slovak Academy of Sciences (grant number 2/1004/21 to I.B.), by the Swiss National Foundation (grant number NF 31-59415.99 to A.E.), the M. E. Müller Foundation of Switzerland and the European Union Quality of Life and Management of Living Resources Project (grant number QLRT-2000-00778 to A.E.).

References

- Adrian, M., Dubochet, J., Fuller, S.D., and Harris, J.R. (1998) Cryo-negative staining. *Micron* **29**: 145–160.
- Backman, K., Ptashne, M., and Gilbert, A.W. (1976) Construction of plasmids carrying the *cl* gene of bacteriophage lambda. *Proc Natl Acad Sci USA* **73**: 4174–4178.
- Ben-Yehuda, S., and Losick, R. (2002) Asymmetric cell division in *B. subtilis* involves a spiral-like intermediate of the cytokinetic protein FtsZ. *Cell* **109**: 257–266.
- Ben-Yehuda, S., Rudner, D.Z., and Losick, R. (2003) RacA,

- a bacterial protein that anchors chromosomes to the cell poles. *Science* **299**: 532–536.
- Bi, E.F., and Lutkenhaus, J. (1991) FtsZ ring structure associated with division in *Escherichia coli*. *Nature* **354**: 161–164.
- de Boer, P.A., Crossley, R.E., Hand, A.R., and Rothfield, L.I. (1991) The MinD protein is a membrane ATPase required for the correct placement of the *Escherichia coli* division site. *EMBO J* **10**: 4371–4380.
- de Boer, P.A., Crossley, R.E., and Rothfield, L.I. (1992) Roles of MinC and MinD in the site-specific septation block mediated by the MinCDE system of *Escherichia coli*. *J Bacteriol* **174**: 63–70.
- Bramhill, D., and Thompson, C.M. (1994) GTP-dependent polymerization of *Escherichia coli* FtsZ protein to form tubules. *Proc Natl Acad Sci USA* **91**: 5813–5817.
- Cha, J.H., and Stewart, G.C. (1997) The divIVA minicell locus of *Bacillus subtilis*. *J Bacteriol* **179**: 1671–1683.
- Daniel, R.A., Harry, E.J., and Errington, J. (2000) Role of penicillin-binding protein PBP 2B in assembly and functioning of the division machinery of *Bacillus subtilis*. *Mol Microbiol* **35**: 299–311.
- Dubochet, J., Adrian, M., Chang, J.-J., Homo, J.-C., Lepault, J., McDowell, A.W., and Schultz, P. (1988) Cryo-electron microscopy of vitrified specimens. *Qu Rev Biophys* **21**: 129–228.
- Edwards, D.H., and Errington, J. (1997) The *Bacillus subtilis* DivIVA protein targets to the division septum and controls the site specificity of cell division. *Mol Microbiol* **24**: 905–915.
- Edwards, D.H., Thomaides, H.B., and Errington, J. (2000) Promiscuous targeting of *Bacillus subtilis* cell division protein DivIVA to division sites in *Escherichia coli* and fission yeast. *EMBO J* **19**: 2719–2727.
- Errington, J., Daniel, R.A., and Scheffers, D.J. (2003) Cytokinesis in bacteria. *Microbiol Mol Biol Rev* **67**: 52–65.
- Flårdh, K. (2003) Essential role of DivIVA in polar growth and morphogenesis in *Streptomyces coelicolor* A3(2). *Mol Microbiol* **49**: 1523–1536.
- Fu, X., Shih, Y.L., Zhang, Y., and Rothfield, L.I. (2001) The MinE ring required for proper placement of the division site is a mobile structure that changes its cellular location during the *Escherichia coli* division cycle. *Proc Natl Acad Sci USA* **98**: 980–985.
- Hamoen, L.W., and Errington, J. (2003) Polar targeting of DivIVA in *Bacillus subtilis* is not directly dependent on FtsZ or PBP 2B. *J Bacteriol* **185**: 693–697.
- Harry, E.J. (2001) Bacterial cell division: regulating Z-ring formation. *Mol Microbiol* **40**: 795–803.
- Harry, E.J., and Lewis, P.J. (2003) Early targeting of Min proteins to the cell poles in germinated spores of *Bacillus subtilis*: evidence for division apparatus-independent recruitment of Min proteins to the division site. *Mol Microbiol* **47**: 37–48.
- Hu, Z., and Lutkenhaus, J. (1999) Topological regulation of cell division in *Escherichia coli* involves rapid pole to pole oscillation of the division inhibitor MinC under the control of MinD and MinE. *Mol Microbiol* **34**: 82–90.
- Lupas, A., Müller, S., Goldie, K., Engel, A.M., Engel, A., and Baumeister, W. (1995) Model structure of the Omp alpha rod, a parallel four-stranded coiled coil from the hyperthermophilic eubacterium *Thermotoga maritima*. *J Mol Biol* **248**: 180–189.
- Margolin, W. (2001) Spatial regulation of cytokinesis in bacteria. *Curr Opin Microbiol* **4**: 647–652.
- Marston, A.L., Thomaides, H.B., Edwards, D.H., Sharpe, M.E., and Errington, J. (1998) Polar localization of the MinD protein of *Bacillus subtilis* and its role in selection of the mid-cell division site. *Genes Dev* **12**: 3419–3430.
- Muchova, K., Kutejova, E., Scott, D.J., Brannigan, J.A., Lewis, R.J., Wilkinson, A.J., and Barak, I. (2002) Oligomerization of the *Bacillus subtilis* division protein DivIVA. *Microbiology* **148**: 807–813.
- Müller, S., Goldie, K.N., Bürki, R., Häring, R., and Engel, A. (1992) Factors influencing the precision of quantitative scanning transmission electron microscopy. *Ultramicroscopy* **46**: 317–334.
- Norris, V., Demarty, M., Raine, D., Cabin-Flaman, A., and Le Sceller, L. (2002a) Hypothesis: hyperstructures regulate initiation in *Escherichia coli* and other bacteria. *Biochimie* **84**: 341–347.
- Norris, V., Misevic, G., Delosme, J.M., and Oshima, A. (2002b) Hypothesis: a phospholipid translocase couples lateral and transverse bilayer asymmetries in dividing bacteria. *J Mol Biol* **318**: 455–462.
- Raskin, D.M., and de Boer, P.A. (1997) The MinE ring: an FtsZ-independent cell structure required for selection of the correct division site in *E. coli*. *Cell* **91**: 685–694.
- Raskin, D.M., and de Boer, P.A. (1999a) MinDE-dependent pole-to-pole oscillation of division inhibitor MinC in *Escherichia coli*. *J Bacteriol* **181**: 6419–6424.
- Raskin, D.M., and de Boer, P.A. (1999b) Rapid pole-to-pole oscillation of a protein required for directing division to the middle of *Escherichia coli*. *Proc Natl Acad Sci USA* **96**: 4971–4976.
- Rowland, S.L., Fu, X., Sayed, M.A., Zhang, Y., Cook, W.R., and Rothfield, L.I. (2000) Membrane redistribution of the *Escherichia coli* MinD protein induced by MinE. *J Bacteriol* **182**: 613–619.
- Shih, Y.-L., Le, T., and Rothfield, L. (2003) Division site selection in *Escherichia coli* involves dynamic redistribution of Min proteins within coiled structures that extend between the two cell poles. *Proc Natl Acad Sci USA* **100**: 7865–7870.
- Stragier, P. (2001) A gene odyssey: exploring the genomes of endospore-forming bacteria. In *Bacillus subtilis and its Relatives: from Genes to Cell*. Sonenshein, A.L., Losick, R., and Hoch, J.A. (eds). Washington, DC: American Society for Microbiology Press, pp. 519–525.
- Thomaides, H.B., Freeman, M., El Karoui, M., and Errington, J. (2001) Division site selection protein DivIVA of *Bacillus subtilis* has a second distinct function in chromosome segregation during sporulation. *Genes Dev* **15**: 1662–1673.
- Whitby, F.G., Kent, H., Stewart, F., Stewart, M., Xie, X., Hatch, V., et al. (1992) Structure of tropomyosin at 9 Ångströms resolution. *J Mol Biol* **227**: 441–452.
- Woldringh, C.L., Mulder, E., Huls, P.G., and Vischer, N. (1991) Toporegulation of bacterial division according to the nucleoid occlusion model. *Res Microbiol* **142**: 309–320.

Wu, L.J., and Errington, J. (2003) RacA and the Soj–Spo0J system combine to effect polar chromosome segregation in sporulating *Bacillus subtilis*. *Mol Microbiol* **49**: 1463–1475.

Zhang, Y., Rowland, S., King, G., Braswell, E., and Rothfield, L. (1998) The relationship between hetero-oligomer formation and function of the topological specificity domain of the *Escherichia coli* MinE protein. *Mol Microbiol* **30**: 265–273.